









Development of AI Controller for Solar /Battery Fed H-Bridge Cascaded Multilevel Converter UPQC under Different Loading Conditions

Koganti Srilakshmi * , N. Yashaswini ** , Sravanthy Gaddameedhi * , Ramprasad Vangalapudi* 
, Praveen Kumar Balachandran *** , Surender Reddy Salkuti **** , M M Fayaz Basha* 

* Department of Electrical and Electronics Engineering, Sreenidhi Institute of Science and Technology, Hyderabad, Telangana, India.

** Department of Mechanical Engineering, Sreenidhi Institute of Science and Technology, Hyderabad, India,

*** Department of Electrical and Electronics Engineering, Vardhaman College of Engineering, Hyderabad, TS 501218, India.

**** Department of Railroad and Electrical Engineering, Woosong University Daejeon, Republic of Korea

(kogantisrilakshmi29@gmail.com, yashaswininandu@gmail.com, sravanthi314@gamil.com, ramprasadgurukul@gmail.com, praveenbala038@gmail.com, surender@wsu.ac.kr)

‡

Corresponding Author: Dr. Koganti Srilakshmi, Sreenidhi Institute of Science and Technology, Tel: +91 8885851666, kogantisrilakshmi29@gmail.com

Received: 09.12.2023 Accepted:27.01.2024

Abstract: This research investigates the application of a H-Bridge cascade five-level Unified Power Quality Conditioner (5L-UPQC) in conjunction with photovoltaic and battery storage systems to address power quality issues. The aim is to address these challenges without the need for complex transformations such as abc , $dq0$, $\alpha\beta$. To achieve this, a control scheme based on artificial neural networks with Levenberg-Marquardt back-propagation training is employed for the H-Bridge cascade 5L-UPQC. This control scheme generates the necessary reference signals for both the shunt and series voltage source converters. Furthermore, a tribrid adaptive neuro-fuzzy controller, combined with Sliding Mode Control (SMC), is proposed to minimize DC link error current. This controller leverages the strengths of both fuzzy logic and artificial neural networks. The primary objective of this proposed scheme is to ensure a constant DC Link capacitor Voltage (DLCV) during load changes, reduce Total Harmonic Distortion (THD) in the source current and load voltage, and effectively eliminates supply voltage fluctuations such as sag/swell and disturbances. The effectiveness of the proposed method is demonstrated through four cases involving various load permutations. To assess the performance of the developed method, a comparison is conducted with two-level and three-level UPQC configurations, as well as existing methods found in the literature.

Keywords- H bridged 5L-Unified Power Quality Conditioner, Total Harmonic Distortion, Voltage source converter, Sag, Disturbance, swell

UPQC	Unified Power quality conditioner	DLCV	Direct current link capacitor voltage
Five-level-UPQC	5L-UPQC		
PV	Photovoltaic	SRF	Synchronous reference frame
BSS	Battery storage system	THD	Total harmonic distortion
PQ	Power Quality	PF	Power factor
ANN	Artificial neural network	GA	Genetic algorithm
LMBP	Levenberg- marquardt back propagation	PSO	Particle swarm optimization
		PIC	Proportional integral controller
p-q	Instantaneous reactive power	SHAPF	Shunt Active Power Filter
		GWO	Grey wolf optimization

PWM	Pulse width modulation	V_{dc}	DC link voltage
BBC	Buck-boost converter	V_{dc}^{ref}	Reference DLCV
SMC	Sliding mode control	i_{sh_abc}	Shunt filter compensated current in abc
FLC	Fuzzy logic controller	Δi_{dc}	DC link output error
VSC	Voltage source converter	$i_{sh_abc}^{ref}$	Shunt filter reference compensated current in abc phases
MSE	Mean square error	i_{dc}^{ref}	Reference DC current
BBO	Biogeography based optimization	R_{se}	SEAF Resistance
SEAF	Series Active Power Filter	$V_{dc, err}$	DLCV error
BC	Boost converter	$i_{BS, er}^*$	Reference battery error current
ACO	Ant colony algorithm	i_{ph}	Photocurrent source
SCC	Short circuit current	L_{sh}	SHAPF Inductance
FOPID	Fractional order proportional integral derivate	i_{BS}^{ref}	Reference current of battery
MSF	Membership function	i_d	Forward diode carrying current
ANFIS	Artificial neuro-fuzzy interface system	$i_{BS, err}$	Battery error current
FF-ANN	Firefly based ANN	$R_{s, PV}$ and $R_{sh, PV}$	Series and parallel cell resistances of PV
PPFFA	Predator-prey firefly algorithm	$i_{sh, PV}$	Parallel current of PV cell
SPG	Solar power generation	i_{PV}	PV cell output current
V_{LL}	Line to Line rms voltage	$i_{PV, m}, V_{PV, m}$	Module current and voltage
CE	Change in error	$i_{s, PV}$	Reverse saturation current
OL	Output Layer of ANN	Q	Electron charge
IL	Input layer of ANN	η	Diode ideal factor
HL	Hidden layer of ANN	k	Boltzmann's constant
E	Error	T_C	Cell temperature
m	Modulation index	N_s	Number of series connected PV cell
$V_{cr, pp}$	Peak-to-peak voltage ripple	G, G_n	Solar irradiance (W/m ²) and at STC
Δi_{imax}	Peak ripple current	ΔT_C	Variation in PV cell temperature
V_m	Peak voltage of the system	P_{PV}	Output PV power
a_f	Overloading factor	P_{BS}	Battery output power
$f_{sh} f_{se}$	Switching frequency	P_{dc}	Power at DC link
L_{se}	SEAF Inductance	$E_{f1,2}(i_t, i_h, i_b)$	No load battery voltage
V_{S_abc}	Source voltage for abc phases	R	Internal resistance of battery
R_S, L_S	Grid Resistance and Inductance	i_b	Battery current
V_{l_abc}	Load voltage for phases a, b, c	E_0	Battery constant voltage
C_{dc}	DC link capacitance	Q	Battery capacity
V_{se_abc}	Series injected voltage for phases a, b, c	$SOCOB$	State of charge of battery
$V_{se_abc}^{ref}$	Reference compensated voltage in abc phase	ΔV_{PV}	Change in PV voltage
i_{S_abc}	Source current for abc phases	Δi_{PV}	Change in PV current
i_{l_abc}	Load current for abc phases		
R_{sh}	SHAPF Resistance		

1. Introduction

In recent years, integrating renewable energy systems like solar and wind into the distribution network has been encouraged to reduce the stress on converters and ratings. The output of a traditional square-wave inverter is a square wave with a significant amount of harmonics. This necessitates the use of large-area filters to tailor the output and create sinusoidal shape. When employing traditional square-wave

inverters, the cost and size of the filter rise, which becomes a significant disadvantage. The admirable properties of multi-level inverters that produce leveled output. Compared to traditional square-wave inverters, leveled output requires smaller filters.

The solar-integrated UPQC was developed to address PQ issues efficiently. In addition, a novel fuzzy-based proportional integral controller was designed for the

Maximum power tracking technique to extract maximum power and balance DLCV [1]. Besides, a new hybrid enhanced method associated with the ANN technique for the SHAPF was introduced to reduce the imperfections in current waveforms and improve the PQ in the distribution network [2]. Next, the PSO and GWO-based optimal SHAPF was designed with the optimal tuning of fractional order proportional integral controller for reactive power and harmonic compensation under the balance and unbalanced loading conditions as case studies with an experimental investigation [3]. However, the performance of wind systems connected to UPQC was studied on different loads and faulty conditions by adopting hysteresis and PWM techniques [4]. Further, the power flow analysis of the UPQC was analysed on a three-phase distribution system with various fault conditions from the point of impedance matching technique [5].

The various existing algorithms for controlling the operation of SHAPF and harmonics isolation techniques, DLCV regulation, and current control methods are discussed [6]. A new metaheuristic HBO was proposed from the intelligent hunting behaviour of honey badgers with a motive for solving optimization problems. Besides, the fuzzy-based hybrid technique was adopted to achieve maximum out of PV. However, to reduce the complexity the ANN was considered for UPQC reference signal generation to solve PQ issues [7]. The intelligent fuzzy-tuned proportional integral controller PIC was designed for the hybrid shunt active and passive filters to minimise the current THD. However, the performance analysis was carried out for varying loads using Clarke's transformation [8]. Meanwhile, by adopting ANN, the Solar PV powered UPQC was presented to reduce grid current THD during voltage fluctuations like sag, and swell. In addition, the proposed method was compared with SRF and reactive power theory methods under varying load conditions [9]. An evolutionary PSO and GWO algorithm was proposed to select optimal Kp, Ki values of the PIC of SHAPF to minimize THD and manage reactive power [10]. However, to regulate DLCV and to handle power feed forward ANN has been suggested for PV/wind associated UPQC [11].

The H bridge inverter-based single phase SHAPF with a modified Predictive Current Control method was introduced to reduce THD in grid current waveform [12]. Future, the microgrid-connected multilevel DSTATCOM was developed to eliminate voltage and current distortions effectively [13]. Future, a comprehensive study was done on various phase synchronization techniques used to control the working of SHAPF [14]. The novel technique was introduced for the UPQC to improve power quality to regulate energy transfer between sources and loads [15].

Intelligent hybrid controllers like fuzzy-PIC and fuzzy proportional integral derivative controllers were proposed for the AC-DC micro-grid system to improve voltage stability and enhance PQ in the presence of D-STATCOM [16]. However, the GWO was suggested to optimize the gain parameters of PIC based UPQC to reduce THD for both linear and non-linear loads [17]. A PIC was adopted to stabilize the DLCV for SHAPF to successfully address PQ problems by adopting hysteresis current control for pulse generation. Additionally,

performance was studied on both linear and non-linear loads [18]. The BBO was selected to obtain optimal gain values of PIC and for fast action in fault identification with higher accuracy with a motive of stabilizing DLCV fluctuations [19].

The hybrid fuzzy ANN control technique has been adopted for UPQC to minimize the current THD and voltage fluctuations and improve network usage [20]. The Improved bat and Moth Flame metaheuristic optimization methods were hybridized to solve the PQ issues by optimal selecting the gain values of PIC [21]. The FLC was developed for SEAF of the distribution network to minimize the current and voltage-related PQ problems [22].

The predator-prey firefly algorithm was selected for the optimal selection of gain parameters of PIC adapted to the SHAPF to reduce the THD and to enhance the PF [23]. A Soccer match optimization for the optimal selection of weights for the ANN controller was suggested for PV/battery-associated UPQC to solve PQ issues [24]. The ACO was chosen for selecting the Kp, Ki values of PIC for the SHAPF to reduce THD under several loading conditions [25]. An adaptive novel hysteresis band with FLC was designed to the PV-associated 9-level VSC based UPQC to receive fluctuations free signals [26]. Next, the Soccer-league optimization was proposed for the optimal selection of PIC gain parameters for UPQC to successfully handle both voltage fluctuations and current distortions [27].

The hybrid control technique with both characteristics of FLC and ANN was recommended to the UPQC to reduce the load side voltage and grid side current waveforms imperfections with DLCV balancing for dynamic loads [28]. The ANN based method was suggested for 5L-UPQC to control the PQ problems [29]. The firefly based optimization was used to train ANNC was developed for the shunt VSC for the PV/battery UPQC to reduce the MSE and minimize THD [30]. The self tuning filter based method was developed for UPQC integrated with renewable sources to address PQ issues [31]. The LMBP-trained ANN controller was adopted for UPQC to mitigate current and voltage-related PQ problems efficiently [32].

It was investigated [33] the advantages and difficulties of integrating renewable energy sources into the system and their control strategies. A few recommendations were also made to transform the conventional grid into a smart grid, and the implications of smart grid technologies on the national grid were underlined [34]. For changes in solar irradiation, the comparison of P & O and PSO algorithms to provide MPP for the PV system was investigated [35]. Integration of renewable sources to micro grid for MPPT was studied with power management [36]. High voltage isolated ACDC converters were developed based on the modular technology [37]. Fuzzy logic controller was suggested for PV-MPPT to improve the overall performance by maximum power point tracking [38].

From the Table-1 literature, it is very clear that most of the literature papers mainly focused on various controllers with the traditional abc-dqo- $\alpha\beta 0$ transformations used in SRF active reactive power theories with PLL and low pass filters with limited objectives. This manuscript develops an ANN based reference signal generation for PV/battery connected

DC link UPQC in addition to ANFIS controller for DC link balancing. The novelty of this manuscript is highlighted in the steps below:

Table 1: Existing Literature

Ref/ year [No]/Year	Control		PQ Issues				Loads	
	Reference signal generation	Controller	THD	DLCV balancing	Supply Voltage sag, swell	Supply Voltage disturbance	Non-linear sensitive load	Unbalanced load
[3] / 2020	p-q theory	FOPID	✓				✓	✓
[4]/ 2022	SRF	PIC	✓					
[7]/ 2023	ANN	ANN	✓	✓	✓	✓	✓	✓
[8]/ 2022	SRF	FUZZY-PI	✓	✓			✓	
[11]/ 2021	ANN	ANN	✓		✓		✓	✓
[19]/ 2021	SRF	PI-BBO	✓		✓		✓	✓
[21]/2021	SRF	ANFIS	✓				✓	✓
[22]/2018	p-q	FUZZY	✓		✓		✓	
[23]/ 2019	SRF	PPFFA	✓				✓	✓
[25]/2019	SRF	PI-ACO	✓				✓	✓
[29]/ 2017	ANN	ANN	✓	✓	✓		✓	✓
[30]/2023	SRF	FF-ANN	✓	✓	✓	✓	✓	✓
Proposed 5L-UPVBES	ANN	ANFIS-SMC	✓	✓	✓	✓	✓	✓

- Developing the H-bridge cascade five level VSC for UPQC for effectively reducing imperfections in waveforms effectively.
- Introducing the LMBP trained ANNC for generating effective reference signals in order to abolish the need of complex abc-dq0- $\alpha\beta 0$ conversions i.e SRF and p-q theories.
- Proposing the tribrid ANFIS and SMC controller to maintain constant DLCV.
- Incorporating the solar PV and battery systems to the DC link of 5L-UPQC to reduce the stress and burden on VSC, supports to meet the load demand, and maintain constant DLCV during load variations.

2. Configuration of Proposed PCI-SBS

- The objective of the proposed system is to diminish the source current THD, and eliminating the grid voltage side troubles like (disturbance, swell, sag etc.)

Additionally, the suggested ANFIS-SMC scheme for 5L-UPQC with PV and BES (5L-UPQC) is examined on 4-test cases for several types of loads and irradiation to show its superior performance. The concert was tested by comparing it with three and two level converters and with SRF and p-q theory. This paper is structured as follows, section2 gives the modeling of 5L-UPQC, Section 3 explains the proposed control scheme, Section 4 demonstrates the results and discussion, and Section 5 concludes the manuscript.

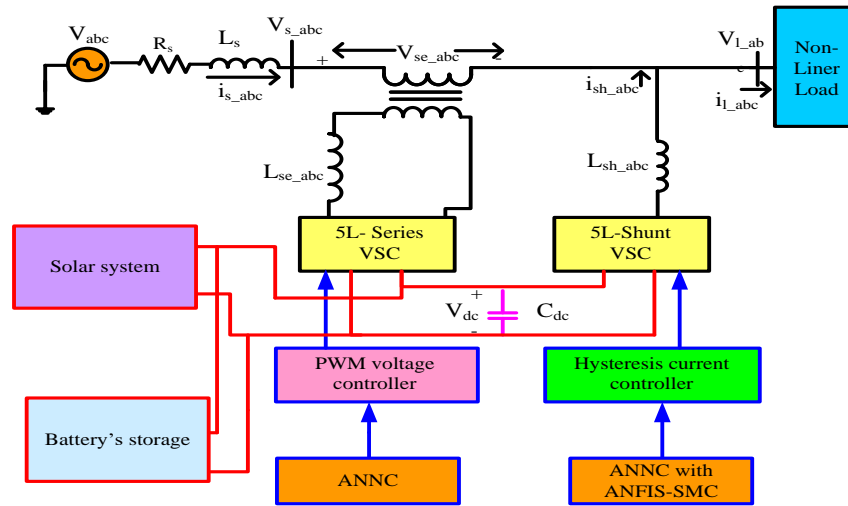


Fig.1. Block diagram of the proposed configuration

Fig. 1 shows the suggested 5L-UPQC setup, in which the DC link of UPQC has been linked to the PV and battery. Combining series and shunt VSCs results in UPQC. With the coupling transformer and inductor, the SAPF aims to solve the grid-side voltage-related issues by providing the appropriate compensating voltage. In a similar way, the grid and the SHAPF are connected via the interface inductance. By introducing an appropriate correcting current, the SHAPF seeks to minimize the settling period and minimize current harmonics while keeping the DLCV constant.

One of the best structures is the multi-level inverter cascaded H-Bridge topology, which requires no clamping tools or components. Although the Cascaded H-Bridge topology's layout is straightforward, more DC sources are needed to power each single H-Bridge cell. Two H-Bridge cells are cascaded into a five-level H-Bridge structure, and every single H-Bridge cell is powered by a DC source. Figure 2 displays a multi-level inverter five-level cascaded H-Bridge arrangement. Fig. 2 also displays the cascaded H-Bridge's 5L voltage output in phase. The five-level output is produced by sequentially triggering power switches as the whole DC link voltage is divided across two H-Bridge cells. Figure 2 shows the power switches used for 5-level Cascaded H-Bridge and its switching order in given in Table 2.

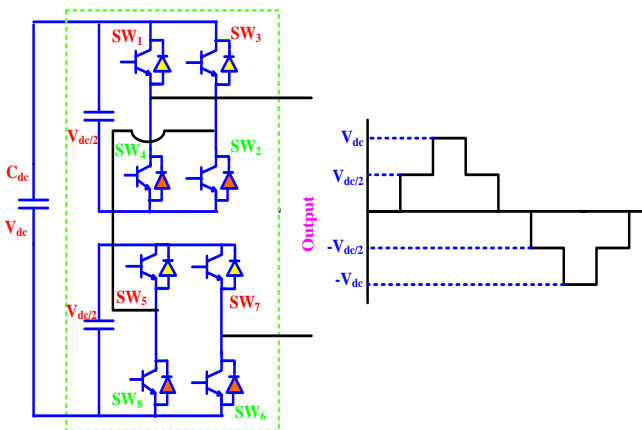


Fig. 2 Proposed 5L-cascade H bridge UPQC with output

2.1 Selection of C_{dc} and V_{dc}

From [29], under faulty conditions, assume the shunt and series VSC's power handling capacities are $0.5XkVA$ and $2XkVA$, respectively. The kVA rating of VSC and V_{dc} is inversely proportional. By the change of 25% of V_{dc} , the equivalent change in the energy across C_{dc} is calculated by Eq. (1)

$$\Delta E_{dc} = 1/2C_{dc} [(1.125V_{dc})^2 - (0.875V_{dc})^2] \quad (1)$$

Assume that for the suppose the load changes from $2XkVA$ to $0.5XkVA$ in 'n' cycles in 'T' sec, then the corresponding change in the system's energy is given by

$$\Delta E_s = (2X - X/2)nT \quad (2)$$

By, equating Eq. (1) and (2), the C_{dc} is given by Eq. (3)

$$C_{dc} = \frac{2(2X - X/2)nT}{(1.125V_{dc})^2 - (0.875V_{dc})^2} \quad (3)$$

Let, V_{dc} is m times to V_m . Where, 'm' modulation index varies between 1.2 and 2. However, %THD depends on L_{sh} and V_{dc} so the value of m is selected as 1.6 [29] for minimum THD. Therefore, V_{dc} is given by Eq. (4)

$$V_{dc} = 1.6 * V_m \quad (4)$$

The V_{dc} for n level converter is evaluated by using [29] Eq. (5)

$$V^{ref}_{dc} = V_{dc} / (n - 1) \quad (5)$$

2.2 Selection of coupling inductors for Shunt and series VSC

The coupling inductors adopted to connect the series and shunt VSC's to the source and the load are limited by di/dt and magnitude of currents. The Δi_{lmax} occurs at $m=0.5$, given in Eq. (6) is controlled by PWM [29].

$$\Delta i_{lmax} = V_{dc} / 6f_{sw}L_{se} \quad (6)$$

Assuming the ripple current is about 10% of the maximum peak-to-peak current given by Eq. (7)

$$\Delta i_{lmax} = 0.1 * i_{lmax} \quad (7)$$

Therefore, the maximum current handling by a series capacitor in terms of power and phase voltage is given by Eq. (8). By using Eq. (6) and (8) Lse can be calculated.

$$i_{max} = \frac{\sqrt{2} * P_r}{3 * V_{ph}} \quad (8)$$

By heuristically testing [29], it has been identified that for m=1.6, V_{refdc}= 700, and L_{sh}= 15 mH the % THD is lower. The value of L_{sh} is given by Eq. (9)

$$i_{max} = \frac{V_{dc}}{4 * h * f_{swmax}} \quad (9)$$

Where, h is the hysteresis band 5-10%.

The solar/battery-fed DC link is proposed for the diode clamped 5L-UPQC. It consists of a hybrid solar and battery energy system to regulate the DLCV during the variation in loads. External support can reduce the converter ratings and stress by lowering the utility's demands. The equation for DC link power demand (P_{dc}) of the suggested technique is given in Eq. (10).

$$P_{PV} + P_{BSS} - P_{dc} = 0 \quad (10)$$

The PV model used in this work was obtained by utilizing the Simulink source. The PV models are connected in series to form a string, and some of such strings are connected in parallel to generate the required amount of voltage and current. The PV cell identifies sun irradiation and converts it into current. The solar output is determined by Eq. (11). The PV cell characteristics for constant temperature and variable irradiation is exhibited in Fig. 4

$$P_{PV} = V_{PV} \times i_{PV} \quad (11)$$

2.3 Battery storage system (BSS)

The BSS provides support in stabilizing the DLCV. Batteries are made up of cells that are placed in series or parallel configurations to produce the desired voltage and current. This work selects Li-ion batteries from the Simuink library due to its advantages like slow discharge and low maintenance cost. The state of charge of battery (SOCOB) is expressed in Eq (12).

$$SOCOB = 50(1 + \int i_{BSS} dtQ) \quad (12)$$

The SPG will decide whether the battery to charge or discharge while satisfying the constraints given by Eq. (13). The discharge of the battery is shown in Fig. 5. The rating selected for solar and battery systems are listed in Appendix. The power flow is shown in Table 3. The control system of solar and battery system fed to DC link is exhibited in Fig.6.

$$SOCOB_{min} \leq SOCOB \leq SOCOB_{max} \quad (13)$$

3. Proposed Control Scheme

Usually, V_{dc} alters during the load fluctuations. However, within a short period of time, the system must return to its initial value in order to become normal. Here, using the

recommended ANNC, the PWM approach generates pulses to the series VSC and hysteresis current controlling for the shunt VSC.

3.1 Shunt Converter

By injecting compensatory current, SHAPF minimizes current signal irregularities and stabilizes DLCV at fault and fluctuating load circumstances. There is an OL, an IL, and an HL in the structure of an ANN. Where the IL gathers the input data and sends it to the HL. It is then multiplied by the corresponding weights on the linked links that connect the IL and HL. In this case, calculations are performed on HL with a chosen bias, and the outcomes are collected in OL.

Table 2: Switches ON/OFF for 5L-Hbridge cascade UPQC

Levelled output voltage	SW1	SW2	SW3	SW4	SW5	SW6	SW7	SW8
V _{dc}	ON	ON	OFF	OFF	ON	ON	OFF	OFF
V _{dc/2}	ON	ON	OFF	OFF	ON	OFF	ON	OFF
0	ON	OFF	ON	OFF	ON	OFF	ON	OFF
-V _{dc/2}	OFF	OFF	ON	ON	ON	OFF	ON	OFF
V _{dc}	OFF	OFF	ON	ON	OFF	OFF	ON	ON

LMBP training for ANN is chosen in this study. To get the intended result, the weights of the link are adjusted during the process of training by analyzing the error. The LMBP training technique is adopted for ANN training where the performance function is MSE. LMBP algorithm uses resulting derivatives for weigh updating, which possesses the characteristics of efficient learning and faster convergence [32]. The LMBP algorithm is an optimization method used to minimize the sum of squared differences between the observed and predicted values in a nonlinear regression problem. It's commonly used for training neural networks with a nonlinear activation function. AI controllers, while powerful and versatile, come with certain limitations like data dependency, over fitting, computational Intensity etc though it helps to take faster and accurate decisions but limited transferability.

Table 3: Power management at DC Link capacitor

Modes of operation	Action taken
Mode-1 : When No SPG	BES only will provide power to P _{DC} .
Mode-2 : When SPG = P _{DC}	Solar PV will supply power P _{DC} .
Mode-3 : When SPG < P _{DC}	The difference sum of the power will be provided by Battery till it reaches SOCB min.
Mode-4 : When SPG > P _{DC}	Excessive solar power is utilized to charge the Battery system till it reaches SOCB max.

3.1.1 ANFIS

The ANFIS is suggested to maintain constant DLCV. The suggested ANFIS is an intelligent hybrid controller with the combination of ANN and Fuzzy logic features. However, for maintaining DLCV constant, the chosen reference DLCV is compared with respect to the obtained DLCV; and its output E, CE is considered as inputs. The inputs fed to the ANNC are initially trained according to the gaussian MSF to produce the best as shown in Fig. 4. ANFIS mainly consists of five layers, the 1st layer (Fuzzification) the outputs of this layer are fuzzy MSF given by Eq. 14 shown in Fig. 6.

$$\mu_{Ai}(x), i = 1,2. \quad (14)$$

$$\mu_{Bj}(y), j = 1,2.$$

Where, μ_{Ai} , μ_{Bj} are the MSF outputs obtained from the 1st layer. The mathematical representation of Gaussian MSF is given by Eq. (15)

$$\mu(x) = e^{-\frac{(x-a)^2}{b}} \quad (15)$$

The Negative-Big (NEB), Zero (ZOE), Negative medium (NEM), Positive small (PES), Positive medium (PEM), Positive Big (PEB), and Negative-Small (NES) are considered as input. MF's inputs are displayed in Fig 5. The fuzzy-rule-base is given in Table 3.

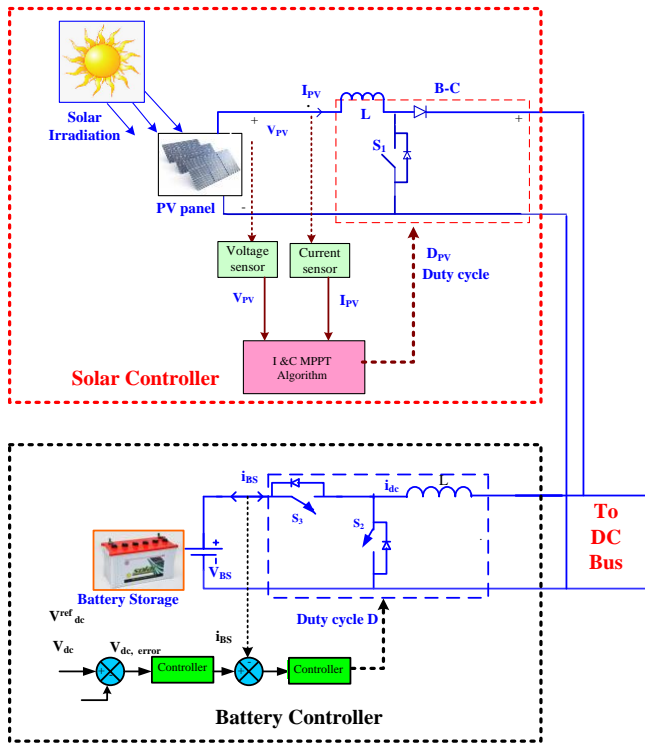


Fig. 3 Control system for external supply sources

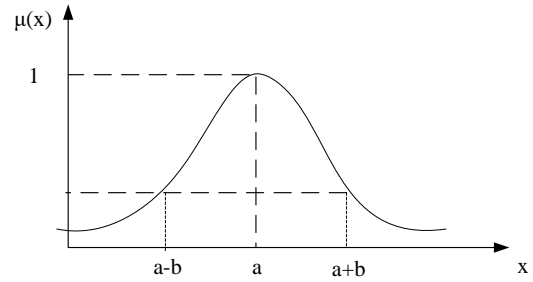
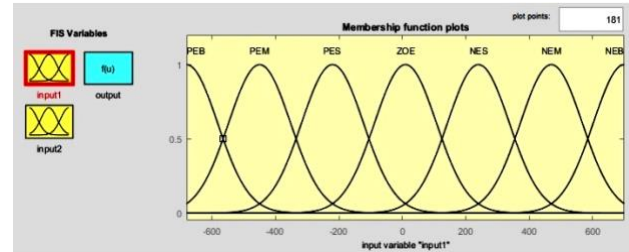
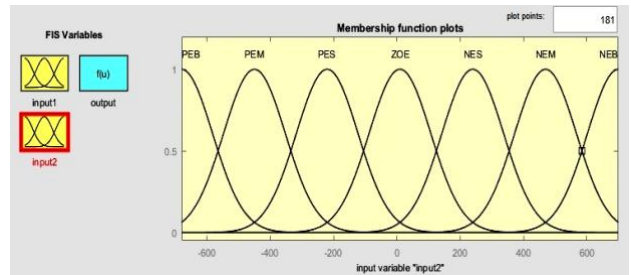


Fig. 4 Gaussian MSF



(a) MF for E



(b) MF for CE

Fig. 5 Fuzzy MFS for E,CE

However, in the 2nd layer (weighting of fuzzy rules) the AND operator is applied, and calculates the firing strength by adopting MSF computed in 1st layer whose output is calculated by Eq. (16).

$$w_k = \mu_{Ai}(x) * \mu_{Bj}(y), i, j = 1,2. \quad (16)$$

The normalization of values takes places in the 3rd layer received from the previous layer. Each node reaches normalization by evaluating the ratio of the kth rule's firing strength (truth values) to the summation of all rule's firing strength is given Eq. (17).

$$\overline{w}_k = \frac{w_k}{w_1 + w_2} \quad k = 1,2. \quad (17)$$

The self-adaptive ability of the ANNC is carried out by applying the inference parameters in the 4th layer (defuzzification) output is given by Eq. (18).

$$\overline{w}_i f_i = \overline{w}_i (p_k u + q_k v + r_k) \quad (18)$$

Lastly, at the 5th layer inputs are get added up to produce the desired total ANFIS output by Eq. (19).

$$f = \sum_i \overline{w}_i f_i \quad (19)$$

Fig.7 shows the block diagram of the proposed ANFIS.

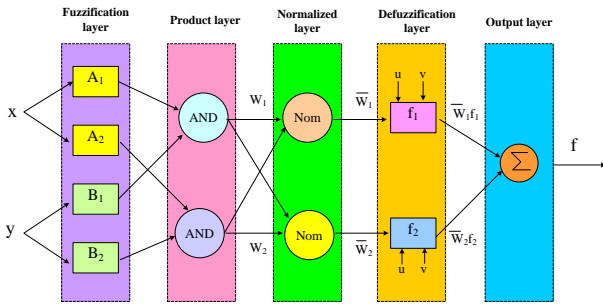


Fig. 6 Structure of ANFIS

3.1.2 Sliding Mode Controller

A sliding mode controller (SMC) is a type of control system used in engineering and control theory to achieve robust and precise control of dynamic systems. It is particularly effective for controlling systems with uncertainties, disturbances, and nonlinearities. The key concept behind the sliding mode control is to create a sliding surface in the state space of the system and drive the system's state trajectory onto this surface and maintain it there. The basic idea of a sliding mode controller can be as follows:

Sliding Surface: A sliding surface is a hyper-plane or a sub manifold in the state space of the system. It is defined depending on the desired behavior of system.

Control Law: The control law is designed such that it drives the system's state onto the sliding surface and maintains it there. The controller's objective is to keep the system's trajectory sliding along this surface.

Sliding Mode: When the system's state lies on the sliding surface, it enters a sliding mode. In this mode, the system's dynamics are simplified, making it easier to control.

Here, Eq. (20) is used to evaluate the error.

$$x_1 = V^{ref}_{dc} - V_{dc} = err(n) \quad (20)$$

The Eq. (21) provides the derivative of the estimated error.

$$x_2 = \frac{1}{T} e(n) - err(n - 1) \quad (21)$$

Here, T is a time period, and x1 and x2 are variables in state space whose expression is Eq. (22)

$$\dot{x} = \begin{bmatrix} \dot{x}_1 \\ \dot{x}_2 \end{bmatrix} = \begin{bmatrix} 0 & 1 \\ 0 & 0 \end{bmatrix} \begin{bmatrix} x_1 \\ x_2 \end{bmatrix} + \begin{bmatrix} 0 \\ -k \end{bmatrix} \mu \quad (22)$$

However, Eqs. (23) and (24) each represent the sliding plane's state space equations.

$$s = [C \quad 1] \begin{bmatrix} x_1 \\ x_2 \end{bmatrix} = Cx_1 + x_2 \quad (23)$$

$$\dot{s} = [C \quad 1] \begin{bmatrix} \dot{x}_1 \\ \dot{x}_2 \end{bmatrix} = C \dot{x}_1 + \dot{x}_2 \quad (24)$$

According to the power rate law,

$$\dot{s} = -L|s|^\alpha \text{sgn}(s) \quad (25)$$

Here,

$$\text{sgn}(s) = \begin{cases} 1 & \text{for } s > 0 \\ -1 & \text{for } s < 0 \end{cases} \quad (26)$$

The Eq. (27) is used to calculate the μ control law.

$$\mu = \frac{1}{K} [Cx_2 + L|s|^\alpha \text{sgn}(s)] \quad (27)$$

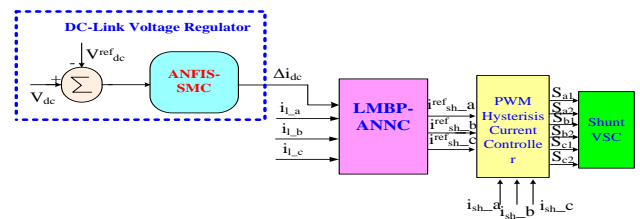


Fig. 7 Shunt Control

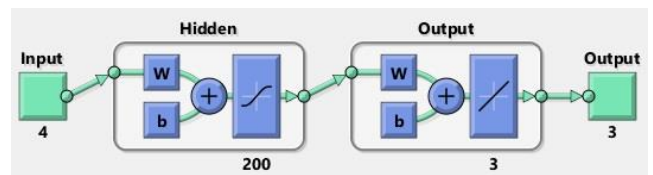


Fig. 8 ANNC based reference current signal generation

The ANFIS with SMC is trained to maintain constant DLCV and to generate reference current signals. However, for keeping the DLCV constant, reference DLCV (V^{ref}_{dc}) is compared with the actual DLCV (V_{dc}) ; its error is chosen as input data, Δi_{dc}. Next, the load currents, like (i_{l_abc}) and DC loss component (Δi_{dc}), are considered as input while the reference currents (i^{ref}_{sh_abc}) are considered as target data as shown in Fig. 7, and the structure with neurons selected are shown in Fig. 8.

3.2 Series VSC

The prominent role of SAPF is to suppress the grid side voltage distortions by injecting the suitable compensating voltage to maintain load side voltage constant. Fig. 9 gives the proposed series converters side reference signal generation scheme and Fig. 10 shows the structure of ANN with a HIL of 200 neurons. The grid side voltages (V_{s_abc}) are regarded as input data to create the reference signals of voltage (V^{ref}_{se_abc}), whereas the reference voltage is regarded as goal data to ANN. PWM generates the gating pulses for series VSC.

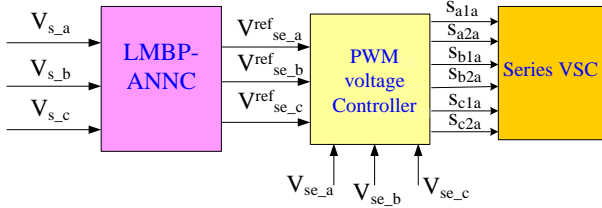


Fig. Fig. 9 Series control

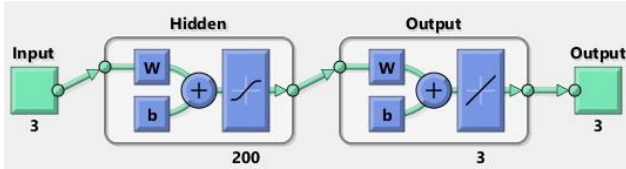


Fig. 10 ANNC for reference voltage generation

4. Results and Discussions

The proposed H-Bridge cascade 5L-UPQC with ANNC was designed in Matlab/ Simulink is specified in Fig 11. The selected system and the UPQC device parameters chosen are presented in appendix and loads selected in this work are listed Table 4. Here, four test cases with various permutations of voltage issues like sag, disturbance, swell, balanced and unbalanced loads with constant irradiation (G) and temperature of 250c were selected to revel the working of developed ANNC on 5L-UPQC is given in Table 5. The voltage related problems like sag, harmonics and swell were selected for both case-1 and 2 and unbalanced grid supply issue is considered for case 3 and 4. However, in this work the reduction of current THD is regarded as objective which is obtained by developed ANN for reference signal generation and optimal selection of shunt and series controller parameters for H-bridge cascade 5L-UPQC. The comparative analysis is carried out with PIC and SMC methods at DLCV balancing. The THD is evaluated by Eq. (28).

$$THD = \frac{\sqrt{(I_2^2 + I_3^2 + \dots + I_n^2)}}{I_1} \quad (28)$$

Where,

In= individual harmonic current distortion values in amps

I1= individual harmonic current distortion values in amps

I2= 2nd harmonic current distortion values in amps

The voltage sag/ swell (Vsag/swell) is evaluated by Eq. (29)

$$V_{sag/swell} = \frac{V_l - V_s}{V_l} = \frac{V_{se}}{V_l} \quad (29)$$

The injected voltage by series filter is calculated by Eq. (30)

$$V_{se} = V_l - V_s \quad (30)$$

The injected current by shunt filter is calculated by Eq. (31)

$$i_{sh} = i_i - i_s \quad (31)$$

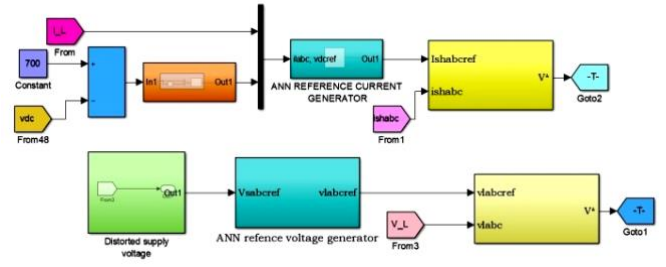


Fig.11 Simulink model of the proposed ANN with ANFIS-SMC

Table 4: Loads Considered

Load1: Balanced 3 Φ nonlinear load: $P_L=3kW, Q_L=0.5$ kVAR
Load 2: Un-balanced load: $P_{La}=3kW, Q_{La}=9$ kVAR; $P_{Lb}=4kW, Q_{Lb}=10$ kVAR; $P_{Lc}=4kW, Q_{Lc}=10$ Kvar
Load 3: Rectifier bridged balanced RL Load: 30ohm & 20mH
Load 4: Unbalanced rectifier RL Load: R_a, R_b, R_c : 10, 20 & 15 ohm; L_a, L_b, L_c : 9.50, 10.52, 18.50 mH

Table 5: Test Cases studies considered for different loads

Condition	Case1	Case2	Case3	Case4
Balanced V_s	✓	✓		
Balanced V_{Sag}, V_{Swell} , disturbance		✓		
Unbalanced V_{Sag}, V_{Swell} , disturbance	✓			
Unbalanced V_s			✓	✓
Current	✓	✓	✓	✓
Constant Irradiation 1000W/m2 and 25 ^o c temperature	✓		✓	
Variable irradiation and 25 ^o c Temperature		✓		✓
DLCV	✓	✓	✓	✓
THD (both V and I)	✓	✓	✓	✓
Load1	✓			
Load 2	✓			
Load 3		✓	✓	
Load 4			✓	✓

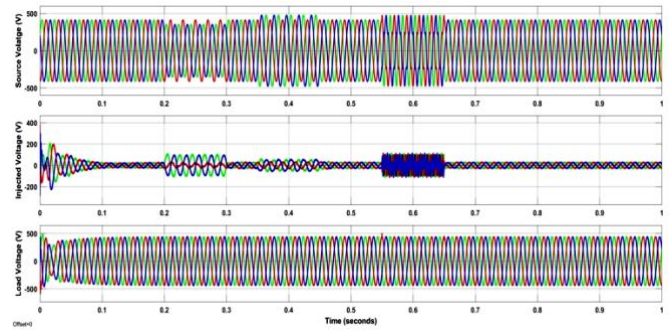
In case1, 30% of unbalanced sag/ swell and a disturbance are created in balanced supply voltage for 0.2 to 0.3 sec, 0.35 to 0.45sec, and 0.5 to 0.6 sec, respectively as shown in Fig 12(a). The developed ANN technique effectively notices the

voltage disputes like dip, raise, and harmonics distortions, supplies the required compensating voltage through the interfacing transformer and maintains the load voltage constant. Besides, to exhibit the behavior of the shunt filter with ANNC, loads 1 and 2 were considered. The load current waveform is unbalanced and non-sinusoidal, as seen in Fig 12(b). The developed method suppresses the distortions in the supply current, reducing the THD of source current to 3.12% and load voltage to 2.12%, much less than other techniques. In addition, it regulates DLCV stable as shown in Fig 12(c) for constant 1000W/ m2 irradiation and 250c of constant temperature.

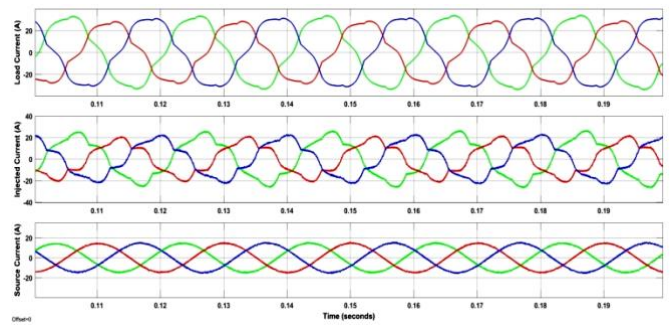
In case 2, similar to case 1, the disturbance is introduced to the 30% of balanced sag and swell. However, the proposed system identifies it successfully and eliminates it by injecting the required compensating voltage, as demonstrated in in Figure 13(a). The load current signal was nonsinusoidal but balanced as shown in Figure 13(b), due to load 3. But, the developed technique reduces the THD of the source current to 2.48% and load voltage to 1.64%, which is lesser than other techniques. However, the exhibited scheme maintains constant DLCV during load as well as irradiation variation, as Figure 13(c) shows.

In case3, unbalanced grid voltage has been supplied with load 3 and 4 acting simultaneously. It is clearly exhibited from the Fig. 14 that proposed system handles imbalances effectively and provides constant balanced voltage to load. Due to the selected load the load currents were observed to be sinusoidal and imbalance in phases. The current THD was reduced to 3.47% and voltage to 2.99%. However, the suggested method maintains constant DLCV. In case 4, the unbalanced grid voltage is selected with load 4, the developed systems eliminates the imperfections in supply voltage and reduces the current THD to 2.96% and voltage THD to 2.14% in addition to maintain DLCV stable during load and irradiation variation as shown in Fig. 19.

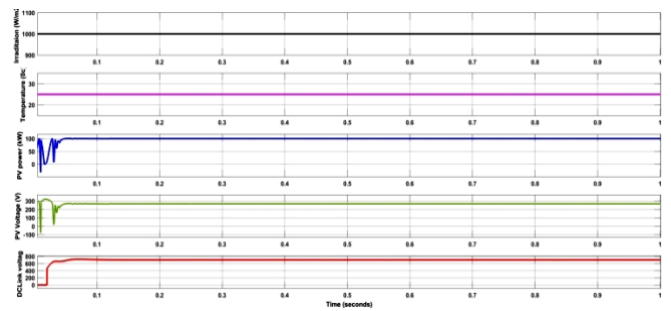
Table 6 compares the THD of the proposed method with those of three and two levels in addition to SRF and d-q theory, and others in the literature survey. It exhibits that the proposed method has much lower THD when compared to other techniques. However, Figure 16 represents the FFT analysis of the current proposed system for case2 phase-a. From the results analysis it is clearly exhibited that the proposed cascade 5L H-Bridge UPQC based ANN controller based reference signal generation technique with ANFIS controller effectively works in reducing imperfections in the waveforms and improves THD in addition to the elimination of complex SRF and p-q transformations. Moreover, it also works well and maintains DLCV stable during load and solar irradiation variations effectively.



(a) V_S, V_{se}, V_L

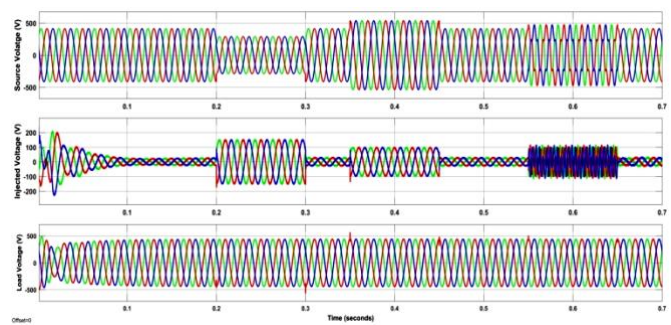


(b) i_L, i_{sh}, i_s



(c) Irradiation, Temperature, PPV, VPV, DLCV

Fig. 12 Waveforms of the developed method for case1



(a) V_S, V_{se}, V_L

(b) i_l, i_{sh}, s

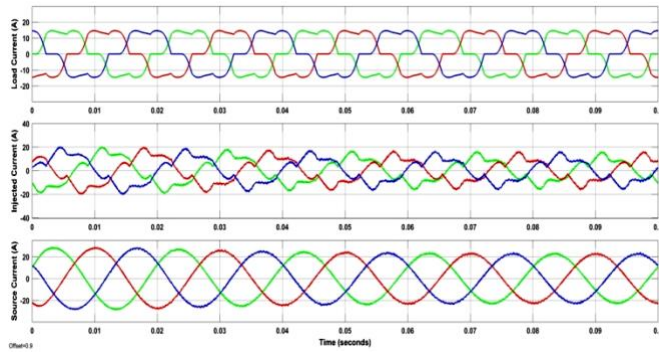
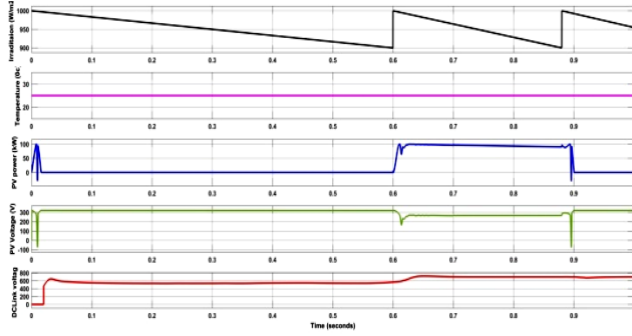


Table 6: THD comparison

Case	Method [Ref]	THD					
		Source Current			Load Voltage		
		Phase-a	Phase-b	Phase-c	Phase-a	Phase-b	Phase-c
1	Proposed Scheme with ANFIS controller	3.12	3.39	3.17	2.12	2.44	2.31
	3L-UPQC with proposed scheme	3.27	3.41	3.25	2.18	2.51	2.46
	2L-UPQC with proposed scheme	3.58	3.81	3.42	2.98	2.84	2.73
	3L-UPQC with SRF theory	3.52	3.87	3.74	3.14	3.07	2.94
	2L-UPQC with p-q theory	3.64	3.91	3.89	3.28	3.13	2.14
	2L-UPQC [29]	5.42	5.43	5.61	4.03	3.86	4.04
	3L-UPQC [29]	4.72	4.45	4.86	3.37	3.27	3.36
	5L-UPQC [29]	3.85	4.09	4.40	3.02	2.97	3.03
	2L-UPQC-SRF [29]	5.47	6.07	5.95	4.45	4.76	4.99
	3L-UPQC-SRF [29]	5.55	6.06	4.94	4.22	4.24	4.43
	5L-UPQC-SRF [29]	4.55	5.45	4.32	3.83	3.98	4.22
2	ANN [7]	3.72	--	--	--	--	--
	Proposed method (ANN with ANFIS)	2.48	2.53	2.62	1.64	2.01	1.98

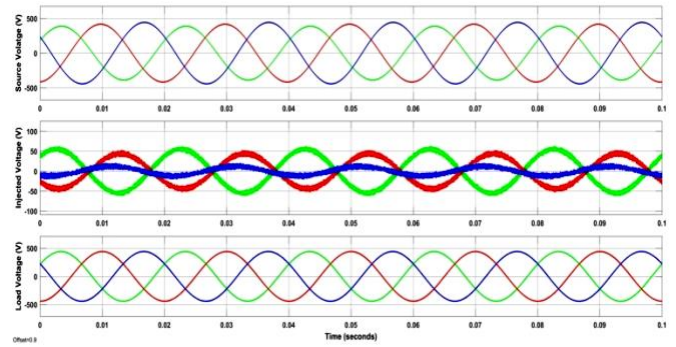
	3L-UPQC with proposed scheme	2.93	2.75	2.64	2.91	2.84	2.73
	2L-UPQC with proposed scheme	3.17	3.05	3.54	3.41	3.22	3.11
	3L-UPQC with SRF theory	3.58	3.12	3.54	3.16	3.35	3.47
	2L-UPQC with p-q theory	4.03	4.26	4.51	4.34	4.12	4.48
	ANN [7] case4	4.55	--	--	--	--	--
	Proposed method	3.47	3.52	4.04	2.99	3.04	3.21
	(ANN with ANFIS)						
3	3L-UPQC with proposed scheme	3.97	3.69	4.17	3.01	3.45	3.67
	2L-UPQC with proposed scheme	4.36	4.21	4.05	3.36	3.71	3.76
	3L-UPQC with SRF theory	4.71	4.62	4.93	3.87	3.68	3.94
	2L-UPQC with p-q theory	4.83	4.78	4.99	4.32	4.57	4.35
	Proposed method	2.96	2.81	2.60	2.14	2.34	2.68
	(ANN with ANFIS)						
4	3L-UPQC with proposed scheme	2.97	2.96	2.86	2.91	2.85	2.77
	2L-UPQC with proposed scheme	3.12	3.58	3.61	3.54	3.67	3.43
	3L-UPQC with SRF theory	4.71	3.67	3.31	3.65	3.68	3.44
	2L-UPQC with p-q theory	4.67	4.97	4.57	4.78	4.27	4.69

Proposed scheme = ANN based reference signal generation

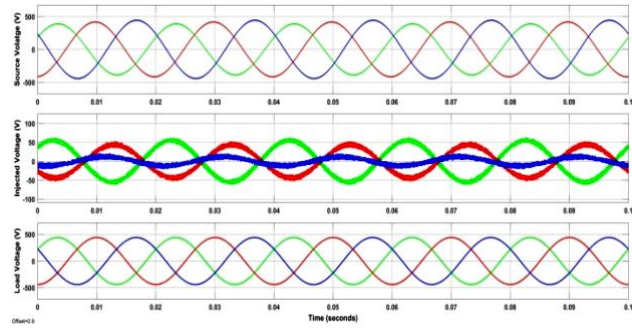


(c) Irradiation, Temperature, P_{PV} , V_{PV} , DLCLV

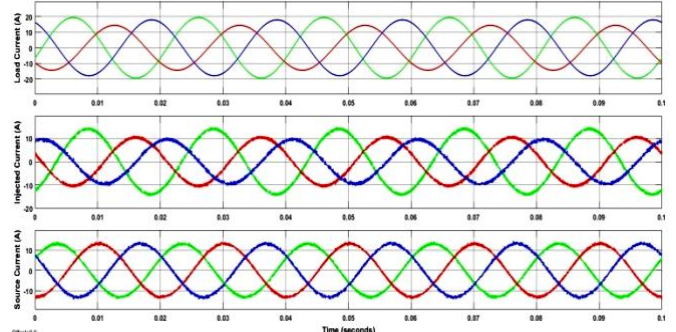
Fig. 13 Waveforms of the developed method for case 2.



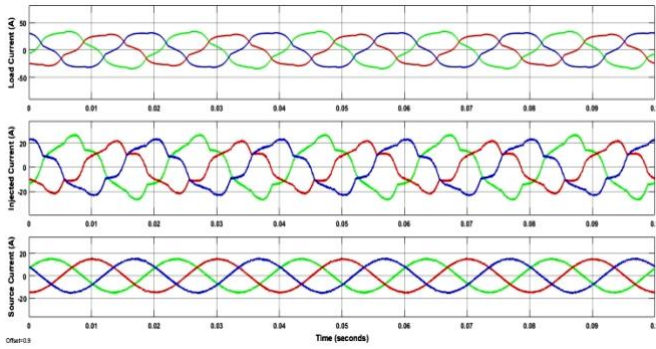
(a) V_S , V_{se} , V_L



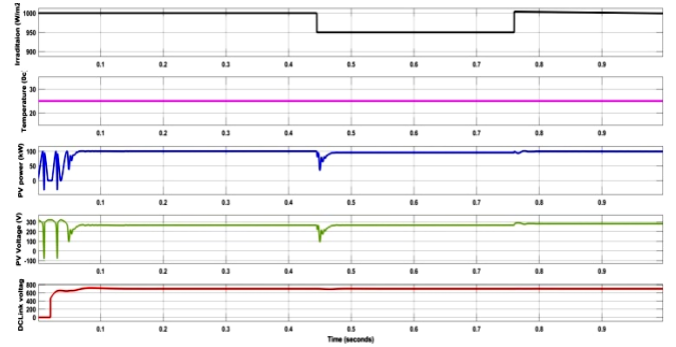
(a) V_S , V_{se} , V_L



(b) i_L , i_{sh} , i_s

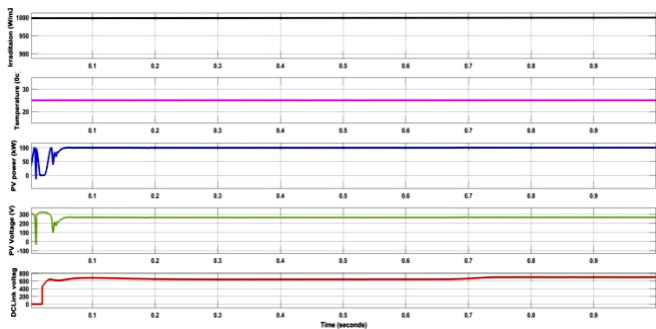


(b) i_L , i_{sh} , i_s



(c) Irradiation, Temperature, P_{PV} , V_{PV} , DLCLV

Fig. 15 Waveforms of the developed method for case 3.



(c) Irradiation, Temperature, P_{PV} , V_{PV} , DLCLV

Fig. 14 Waveforms of the developed method for case 3.

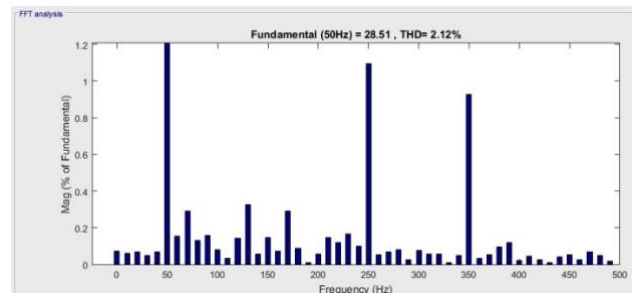


Fig. 16 Current THD spectrum for case2 phase-a

5. Conclusion

This paper proposes an ANNC-based new method for a solar battery connected to UPQC. The LMBP-trained ANN controller is presented to produce the required reference signals for shunt series VSC's to avoid the traditional abc-dq0- $\alpha\beta$ conversions. In addition, the ANFIS hybrid controller is adapted for DLCV balancing. However, the developed H

bridge cascade 5L-UPQC maintains constant DLCV during loads variations, suppresses the source current and load voltage harmonics and improves the current and voltage waveform's shape, and eliminates the fluctuations of supply voltage (disturbance, sag and swell). The comparison is carried out with ANN, PIC and SMC controllers for DLCV balancing and other methods available in the literature. The results of the two test cases show that the developed method provides much lower THD than other methods in literature and within acceptable levels. The developed method can be carried out using metaheuristic optimization control scheme in the future in addition to the micro-grid.

Appendix-1: Test system specifications

The system values are: PCC line voltage: 415 V, 50 Hz; R_s : 0.1ohm, L_s : 0.15 ohm; DC-bus Voltage: 700 V; DC-bus Capacitor: 2200 μ F; Interfacing Inductor of Shunt and series VSC: 6mH, 15mh; Interfacing capacitor of Series VSC: 60 μ F; PV ratings: Rated Power: 214.92w, OCC: 39.8w; SCC: 5.8A, Maximum voltage and current: 39.8V/5.4A, Parallel and series connected PV cells: 11/18; Battery: Rated capacity: 25Ah, Cut off voltage: 487V.

References

1. Dongsheng Yang ,Zhanchao Ma , Xiaoting Gao , Zhuang Ma, Enchang Cui, Control Strategy of Intergrated Photovoltaic-UPQC System for DC-Bus Voltage Stability and Voltage Sags Compensation, *Energies* 2019, 12.
2. Ganesan Arunsankar, Subbaraman Srinath, Optimal controller for mitigation of harmonics in hybrid shunt active power filter connected distribution system: An EGOANN technique, *Journal of Renewable and Sustainable Energy*, Vol. 11, April-2019.
3. Alok Kumar Mishra , Soumya Ranjan Das , Prakash K. Ray ,Ranjan Kumar Mallick, Asit Mohanty Dillip .K. Mishra, PSO-GWO Optimized Fractional Order PID Based Hybrid Shunt Active Power Filter for Power Quality Improvements, *IEEE Access*, Vol.8, pp. 74497 - 74512, May-2020
4. DheyaaIed Mahdi 1 and GoksuGorel2, Design and Control of Three-Phase Power System with Wind Power Using Unified Power Quality Conditioner, *Energies* 2022, 15, 7074.
5. Xiaojun Zhao, Xiuhui Chai, Xiaoqiang Guo, Ahmad Waseem, Xiaohuan Wang and Chunjiang Zhang, Impedance Matching-Based Power Flow Analysis for UPQC in Three-Phase Four-Wire Systems, *Energies* 2021, 14, 2702.
6. Yap Hoon, Mohd Amran MohdRadzi, MohdKhair Hassan, Nashiren Farzilah Mailah, Control Algorithms of Shunt Active Power Filter for Harmonics Mitigation: A Review, *Energies*, Vol.10, No.12, 2038, Dec-2017.
7. Koganti Srilakshmi, K. Krishna Jyothi, G. Kalyani & Y. Sai Prakash Goud. Design of UPQC with Solar PV and Battery Storage Systems for Power Quality Improvement. *Cybernetics and Systems: An International Journal*, March-(2023).
8. Tzu-Chiao Lin ,BawokeSimachew, Intelligent Tuned Hybrid Power Filter with Fuzzy-PI Control, *Energies* 2022, 15, 4371.
9. Okech Emmanuel Okwako1 , Zhang-Hui Lin, Mali Xin 1, Kamaraj Premkumar 2, Alukaka James Rodgers 1, Neural Network Controlled Solar PV Battery Powered Unified Power Quality Conditioner for Grid Connected Operation, *Energies* 2022, 15, 6825.
10. Alok Kumar Mishra, Soumya Ranjan Das, Prakash K. Ray, Ranjan Kumar Mallick, Asit Mohanty , Dillip K. Mishra, PS-O-GW-O Optimized Fractional Order PID Based Hybrid Shunt Active Power Filter for Power Quality Improvements, *IEEE Access*, Vol. 8, pp. 74497 – 74512, April-2022.
11. Kumar Chandrasekaran, Jaisiva Selvaraj, Clement Raj Amaladoss, LogeshwariVeerapan, Hybrid renewable energy based smart grid system for reactive power management and voltage profile enhancement using artificial neural network, *Energy Sources, Part A: Recovery, Utilization, and Environmental Effects*, 2021, Vol. 43, No. 19, pp. 2419–2442.
12. BelqasemAljafari, Kanagavel Rameshkumar, Vairavasundaram Indragandhi, Selvamathi Ramachandran, A Novel Single-Phase Shunt Active Power Filter with a Cost Function Based Model Predictive Current Control Technique, *Energies* 2022, 15, 4531.
13. Krishna Sarker, Debashis Chatterjee & S. K. Goswami, A modified PV-wind-PEMFCS-based hybrid UPQC system with combined DVR/STATCOM operation by harmonic compensation, *International Journal of Modeling and Simulation*, Vol.41, No.4, pp. 243-255, March 2020.
14. Yap Hoon, Mohd Amran Mohd Radzi, Muhammad Ammirul Atiqi Mohd Zainuri, Mohamad Adzhar Md Zawawi , Shunt Active Power Filter: A Review on Phase Synchronization Control Techniques, *Electronics* 2019, 8, 791.
15. Andrzej Szromba, the Unified Power Quality Conditioner Control Method Based on the Equivalent Conductance Signals of the Compensated Load, *Energies* 2020, 13.
16. Abdelnasser A. Nafeh , Aya Heikal , Ragab A. El-Sehiemy, Waleed A.A. Salem, Intelligent fuzzy-based controllers for voltage stability enhancement of AC-DC micro-grid with D-STATCOM, Vol.61, No. 3, pp. 2260-2293, March-2022.
17. Marcel Nicola, Claudiu-Ionel Nicola, Dumitru Sacerdoțianu and Adrian Vintilă, Comparative Performance of UPQC Control System Based on PI-GWO, Fractional Order Controllers, and Reinforcement Learning Agent, *Electronics* 2023, 12, 494.
18. Amir A. Imam, R. Sreerama Kumar, Yusuf A. Al-Turk, Modeling and Simulation of a PI Controlled Shunt Active Power Filter for Power Quality Enhancement Based on P-Q Theory, *Electronics* 2020, 9, 637.
19. Sayed,J.A.; Sabha, R.A.; Ranjan, K.J. Biogeography based optimization strategy for UPQC PI tuning on full order adaptive observer based control. *IET Generation, Transmission & Distribution* 2021, 15, 279-293.
20. Renduchintala, UK,Pang, C,Tatikonda, KM,Yang, L.ANFIS-Fuzzy logic based UPQC in interconnected microgrid distribution systems: modeling, simulation and implementation. *J Eng*.2021; 2021:6–18.
21. Rajesh, P.; Shajin, F.H.; Umasankar, L. A Novel Control Scheme for PV/WT/FC/Battery to Power Quality Enhancement in Micro Grid System: A Hybrid Technique.

- Energy Sources, Part A: Recovery, Utilization, and Environmental Effects 2021, 1-18.
22. Pazhanimuthu, C.; Ramesh, S. Grid integration of renewable energy sources (RES) for power quality improvement using adaptive fuzzy logic controller based series hybrid active power filter (SHAPF), *Journal of Intelligent & Fuzzy Systems* 2018, 35, 749–766.
 23. SahithullahMahaboob, Senthil Kumar Ajithan, SasikalaJayaraman, Optimal design of shunt active power filter for power quality enhancement using predator-prey based firefly optimization, *Swarm and Evolutionary computation*, Vol 44, 522-533, (2019).
 24. KogantiSrilakshmi, CanavoyNarahari Sujatha, Praveen Kumar Balachandran, Lucian Mihet-Popa, and Naluguru Udaya Kumar, “Optimal Design of an Artificial Intelligence Controller for Solar-Battery Integrated UPQC in Three Phase Distribution Networks”, *Sustainability*, Vol. 14, No. 21, Oct-2022.
 25. Aruchamy Sakthivel, P. Vijayakumar, A. Senthilkumar, L. Lakshminarasimman, S. Paramasivam: Experimental investigations on ant colony optimized pi control algorithm for shunt active power filter to improve power quality. *Control Engineering Practice*. (42), 153-169 (2015).
 26. Hassan Kenjrawy, Carlo Makdisie, IssamHoussamo, Nabil Mohammed, New Modulation Technique in Smart Grid Interfaced Multilevel UPQC-PV Controlled via Fuzzy Logic Controller, *Electronics* 2022, 11, 919.
 27. Koganti Srilakshmi ,Nakka Srinivas , Praveen Kumar Balachandran , Jonnala Ganesh Prasad Reddy, Sravanthy Gaddameedhi, NagarajuValluri, ShitharthSelvarajan, Design of Soccer League Optimization Based Hybrid Controller for Solar-Battery Integrated UPQC, *IEEE Access*, Vol. 10, pp. 107116-107136, 2022.
 28. Srilakshmi Koganti , Krishna Jyothi Koganti and Surender Reddy Salkuti , Design of Multi-Objective-Based Artificial Intelligence Controller for Wind/Battery-Connected Shunt Active Power Filter, *Algorithms*, Vol. 15, No. 8, pp. 256, 2022.
 29. SudheerVinnakoti, Venkata Reddy Kota, Implementation of artificial neural network based controller for a five-level converter based UPQC, *Alexandria Engineering Journal*, Elsevier, Vol 57, Issue 3, 2017, pp.1475-1488.
 30. Alapati Ramadevi , Koganti Srilakshmi , Praveen Kumar Balachandran ,Ilhami Colak , C. Dhanamjayulu , and Baseem Khan. Optimal Design and Performance Investigation of Artificial Neural Network Controller for Solar- and Battery-Connected Unified Power Quality Conditioner. *International Journal of Energy Research*, Vol. 2023, 3355124, 22 pages, April-(2023).
 31. M.A.Mansoor, K. Hasan, M.M. Othman, S. Z. B. M. Noor, and I.Musirin. Construction and performance investigation of three phase solar PV and battery energy storage system integrated UPQC. *IEEE Accesses* , Vol.8, 103511 – 103538,
 32. Zhou Ming; Wan Jian-Ru; Wei Zhi-Qiang; Cui Jian, Control Method for Power Quality Compensation Based on Levenberg-Marquardt Optimized BP Neural Networks, 2006 CES/IEEE 5th International Power Electronics and Motion Control Conference.
 33. F. Ayadi; I. Colak; I. Garip, H. Bulbul, “Impacts of Renewable Energy Resources in Smart Grid”, 8th International Conference on Smart Grid, Paris, pp. 183-188, June 2020.
 34. I. Colak; R. Bayindir, S. Sagiroglu, “The Effects of the Smart Grid System on the National Grids”, 8th International Conference on Smart Grid, Paris, pp. 122-126, June 2020.
 35. S. Jaber, A. M. Shakir, “Design and Simulation of a Boost-Microinverter for Optimized Photovoltaic System Performance”, *International Journal of Smart Grid*, Vol. 5, No. 2, pp. 1-9, June 2021.
 36. S. S. Dash, “Tutorial 1: Opportunities and challenges of integrating renewable energy sources in smart” 6th International Conference on Renewable Energy Research and Applications , San Diego, CA, USA, 5-8 Nov. 2017.
 37. M. Tsai, C. Chu, W. Chen, “Implementation of a Serial AC/DC Converter with Modular Control Technology”, 7th International Conference on Renewable Energy Research and Applications, Paris, France, pp. 245-250, Oct. 2018.
 38. A. Belkaid, I. Colak, K. Kayisli, R. Bayindir, Improving PV System Performance Using High Efficiency Fuzzy Logic Control, 8th International Conference on Smart Grid, Paris, pp.152-156, June 2020.